AGU PUBLICATIONS

Geophysical Research Letters

RESEARCH LETTER
10.1002/2014GL059222

Special Section:
Early Results from the Van Allen Probes

Simulated magnetopause losses and Van Allen Probe flux dropouts

M. K. Hudson[1], D. N. Baker[2], J. Goldstein[3,4], B. T. Kress[1], J. Paral[1], F. R. Toffoletto[5], and M. Wiltberger[6]

[1]Physics and Astronomy Department, Dartmouth College, Hanover, New Hampshire, USA, [2]Laboratory for Atmospheric and Space Physics, University of Colorado, Boulder, Colorado, USA, [3]Southwest Research Institute, San Antonio, Texas, USA, [4]University of Texas San Antonio, San Antonio, Texas, USA, [5]Physics and Astronomy Department, Rice University, Houston, Texas, USA, [6]High Altitude Observatory, NCAR, Boulder, Colorado, USA

Abstract Three radiation belt flux dropout events seen by the Relativistic Electron Proton Telescope soon after launch of the Van Allen Probes in 2012 (Baker et al., 2013a) have been simulated using the Lyon-Fedder-Mobarry MHD code coupled to the Rice Convection Model, driven by measured upstream solar wind parameters. MHD results show inward motion of the magnetopause for each event, along with enhanced ULF wave power affecting radial transport. Test particle simulations of electron response on 8 October, prior to the strong flux enhancement on 9 October, provide evidence for loss due to magnetopause shadowing, both in energy and pitch angle dependence. Severe plasmapause erosion occurred during ~14 h of strongly southward interplanetary magnetic field B_z beginning 8 October coincident with the inner boundary of outer zone depletion.

Key Points:
- Simulations of electron flux 8 Oct 2012 produce dropout into L~5.8
- Magnetopause compression bounding the September storage ring formation modeled
- Model shows effects of magnetopause inward motion and ULF waves on electrons

Supporting Information:
- Readme
- Auxiliary Material

Correspondence to:
M. K. Hudson,
Mary.K.Hudson@Dartmouth.EDU

Citation:
Hudson, M. K., D. N. Baker, J. Goldstein, B. T. Kress, J. Paral, F. R. Toffoletto, and M. Wiltberger (2014), Simulated magnetopause losses and Van Allen Probe flux dropouts, *Geophys. Res. Lett.*, *41*, 1113–1118, doi:10.1002/2014GL059222.

Received 16 JAN 2014
Accepted 24 JAN 2014
Accepted article online 29 JAN 2014
Published online 22 FEB 2014

1. Introduction

The extreme variability of outer zone electrons has been confirmed during the first 40 days of operation of the Van Allen Probes satellites launched 30 August 2012 [*Baker et al.*, 2013a]. In order to gain a quantitative understanding of relativistic electron variability, it is necessary to understand both acceleration and loss mechanisms [*Summers et al.*, 2004, 2007]. *Hudson et al.* [2008, 2012] review acceleration by radial transport in storms driven by coronal mass ejections and corotating interaction regions, respectively, while *Shprits et al.* [2008a, 2008b] compare our understanding of such first-invariant conserving processes with local acceleration and loss mechanisms for relativistic electrons in the radiation belts. The extreme variability of outer zone radiation belt electron flux is controlled by competition between source and loss processes [*Selesnick and Blake*, 2000; *Reeves et al.*, 2003]. Whistler mode chorus waves are seen to be both an important acceleration and loss mechanism outside the plasmapause, particularly on the dawnside, while hiss dominates losses inside the plasmasphere [*Thorne*, 2010]. Electromagnetic ion cyclotron waves are thought to be a major loss mechanism on the duskside within the outer plasmasphere and plume region [*Summers and Thorne*, 2003]. Acceleration can occur through energy diffusion [*Summers et al.*, 2007; *Li et al.*, 2007], while losses occur due to pitch angle scattering into the loss cone [*Bortnik et al.*, 2006; *Millan and Thorne*, 2007; *Shprits et al.*, 2008b] and loss to the magnetopause [*Turner et al.*, 2012]. Losses to the Earth's atmosphere are known to be important inside geosynchronous orbit [*Lorentzen et al.*, 2000; *Millan et al.*, 2002, 2007; *O'Brien et al.*, 2004]. In some cases, losses may wipe out the entire radiation belt outer zone over the timescale of a few hours during the main phase of a storm [*Selesnick*, 2006], indicating that the relativistic electron population must be replenished in a day or less. This paper focuses on outer zone depletion observed at the beginning of three geomagnetic storms. Model results are compared with observations from the Van Allen Probes satellites, providing the most complete suite of measurements to date optimized to study the complex processes governing the dynamics of the radiation belts.

2. Observations

Three geomagnetic storms occurring during the first 40 days of postlaunch operation of the Van Allen Probes allow for the examination of prompt losses of multi-MeV outer zone electrons. Figure 1 shows the flux measured by the Relativistic Electron-Proton Telescope (REPT) in the energy range 4–5 MeV [*Baker et al.*, 2013b; see Figure 1, *Baker et al.*, 2013a, for other energies] against the vertical axis L-parameter, the distance in Earth radii (R_E) at which magnetic field lines cross the magnetic equatorial plane using the OP77Q magnetic field model. The horizontal axis shows time from 1 September to 10 October 2012. The black curve

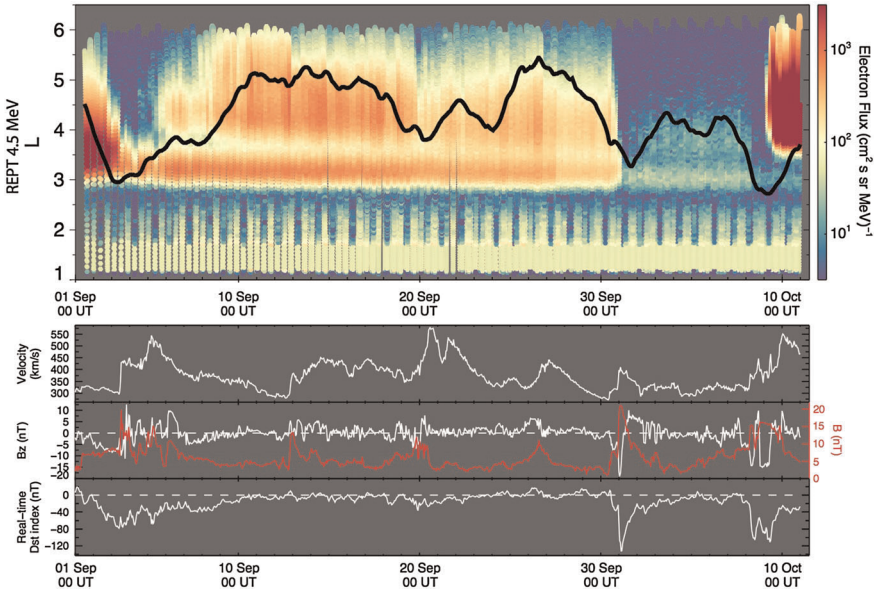

Figure 1. Energetic electron data from the Van Allen Probe satellites showing (a) flux measured by the Relativistic Electron-Proton Telescope in color in the energy range 4–5 MeV [see *Baker et al*., 2013a, Figure 1 for other energies] against the vertical axis OP77Q L-parameter. The horizontal axis is time from 1 September to 10 October 2012. The black curve shows the 2-day averaged plasmapause (outer boundary) derived from a model [*Goldstein et al*., 2005a, 2005b]. Results show a strong enhancement in relativistic electron flux on 9 October following recovery from dropout on 7–8 October. (b) Measured solar wind speed upstream of the Earth's magnetosphere and (c) interplanetary magnetic field mapped to the approximate magnetopause. (d) Geomagnetic activity index Dst.

shows the 2-day averaged plasmapause L-shell derived from a model [*Goldstein et al*., 2005a, 2005b, 2012] bench marked against plasma wave measurements on the Van Allen Probes after wave measurements became available. Extending the plasmapause-data comparison through the strong 8–9 October storm interval shows a strong enhancement in relativistic electron flux on 9 October following recovery from a dropout on 8 October, with weaker dropouts evident on 3–4 September and ~1 October. The concurrently measured solar wind speed and interplanetary magnetic field (IMF) strength upstream of the Earth's magnetosphere are plotted. These data as well as the solar wind density and temperature are used as input to the Lyon-Fedder-Mobarry MHD code [*Lyon et al*., 2004] that has been coupled with the Rice Convection Model (RCM) [*Pembroke et al*., 2012]. The RCM model incorporates drift physics and a more accurate representation of the ring current for stronger storms. The geomagnetic activity index Dst for this period is also plotted. The radiation belt electron behavior was closely related to the solar wind forcing evident in Figure 1, including the long lived "storage ring" between storms at the beginning and end of September, as described further in *Baker et al*. [2013a].

This paper focuses on flux dropouts associated with inward incursions of the magnetopause evident in the MHD simulations described herein and clearly seen in geosynchronous measurements by the GOES spacecraft for all three storms (at http://swpc.noaa.gov). It is remarkable how quickly the magnetosphere recovered from the strong flux dropout evident in the third storm, indicating that the inner magnetosphere is able to effectively reboot from a *tabula rasa* when strongly driven. The MHD simulations driven by upstream solar wind parameters have been analyzed both for magnetopause location and distribution of ULF wave power in frequency and radial distance in the SM equatorial plane perpendicular to the Earth's dipole axis. ULF waves with periods comparable to the electron drift time affect radial transport and energization of radiation belt electrons [*Schulz and Lanzerotti*, 1974; *Elkington et al*., 2003] and have been correlated with changes in radiation belt electron fluxes in numerous studies, c.f. *Rostoker et al*. [1998] and *Loto'aniu et al*. [2010]. Their contribution to radial loss when the nominal outward radial gradient in electron phase space density is inverted, following a coronal mass ejection (CME) shock event, has been suggested [*Shprits et al*., 2006; *Ukhorskiy et al*., 2006, 2009]. The combination of a sudden drop in flux with inward motion of the magnetopause along with enhanced outward radial diffusion due to enhanced ULF wave power, produced by magnetopause compression, may explain radial losses well inside geosynchronous orbit. The dynamics of the global magnetospheric

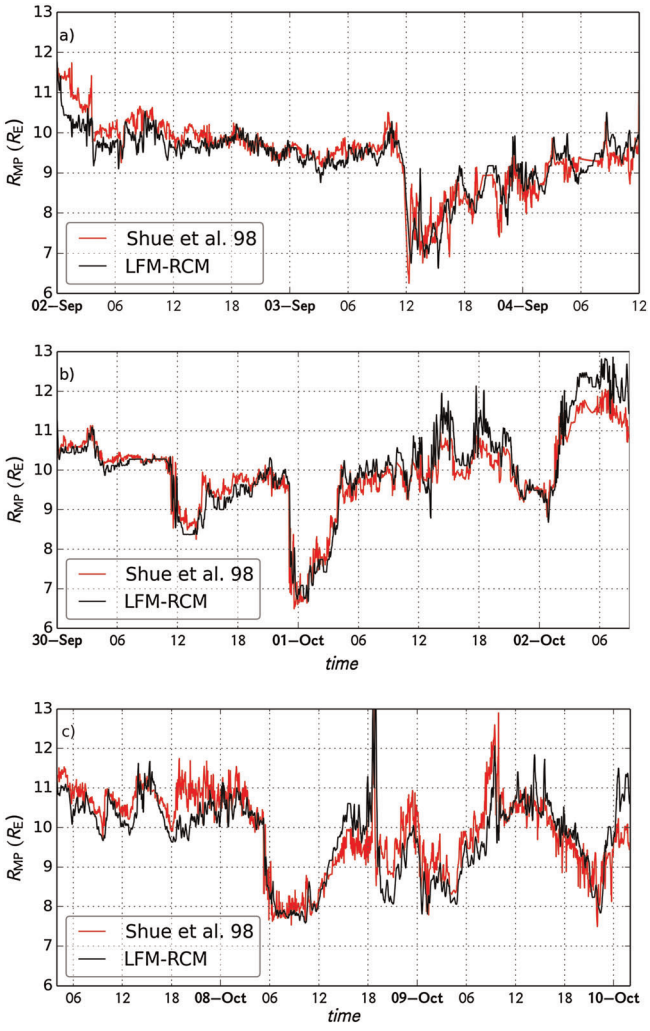

Figure 2. Magnetopause location computed from Lyon-Fedder-Mobarry-Rice Convection Model (LFM-RCM) compared with *Shue et al.* [1998] empirical magnetopause model for (a) the first storm interval 2–4 September 2012; Figures 2b and 2c are LFM-RCM magnetopause comparisons for second and third storms with stronger Dst, see Figure 1d. A 30s LFM output cadence was used for MHD variables.

configuration, including inductive electric field effects on the plasmasheet electron source population [*Kress et al.*, 2014], is key to understanding acceleration by both radial transport [*Hudson et al.*, 2012] and magnetopause losses [*Turner et al.*, 2012, 2013].

3. Simulation Tools

A very simple plasmapause test particle (PTP) simulation is employed to produce the black curve in Figure 1. This model has proven to be successful in reproducing IMAGE observations to within 0.2 to 0.5 R_E [*Goldstein et al.*, 2005a, 2005b]. The PTP model represents the time-varying global plasmapause as an ensemble of cold test particles subject only to E×B drift. The time-varying Volland-Stern convection electric (E) field is driven by solar wind data and the *Kp* geomagnetic index is used as input to a Sub-Auroral Polarization Stream model. The simulation was run with a 12-min time step, starting at 0000 UT on 1 September 2012 and ending at 2400 UT on 10 October 2012. The model-predicted plasmapause location was extracted with an hourly time cadence, at the midnight meridian. A 2-day running (boxcar) average was computed from this hourly midnight plasmapause radial position, to yield the black curve shown in Figure 1. Preliminary work using plasma wave measurements [*Kletzing et al.*, 2013] show good general agreement between the plasma-wave-derived and model-predicted plasmapause locations [*Goldstein et al.*, 2012] beginning 14 September 2012 when the wave measurement was enabled.

Solar wind data from the ACE or WIND satellites are used as input to the Lyon-Fedder-Mobarry (LFM) global MHD model [*Lyon et al.*, 2004], advancing the ideal MHD equations on a nonuniform grid optimized to resolve magnetospheric boundaries. Fields at the inner boundary (a sphere at 2.2 geocentric Earth radii) are mapped from a Poisson solver used to compute potential electric fields in the ionosphere using an empirical model for the ionospheric conductance, based on the F10.7 flux and auroral precipitation [*Wiltberger et al.*, 2009] implemented with the Magnetosphere Ionosphere Coupler, or MIX [*Merkin and Lyon*, 2010]. The LFM-MIX code has been coupled to the Rice Convection Model [*Pembroke et al.*, 2012]. Coupling with the RCM model includes drift physics representation of the ring current, pushing the LFM boundary outward due to increased pressure incorporated from RCM into LFM, and providing a better representation of magnetopause location for stronger Dst storms [*Pembroke et al.*, 2012], see supporting information. Figure 2a compares the magnetopause location computed from LFM-RCM with the *Shue et al.* [1998] empirical model for the first storm interval 3–4 September, where the storage ring feature in Figure 1 at L = 3–3.5 is defined from the residual outer zone following magnetopause erosion [*Baker et al.*, 2013a]. The LFM-RCM simulation was conducted in SM coordinates, and the calculation of magnetopause distance is along the SM *x* axis perpendicular to the

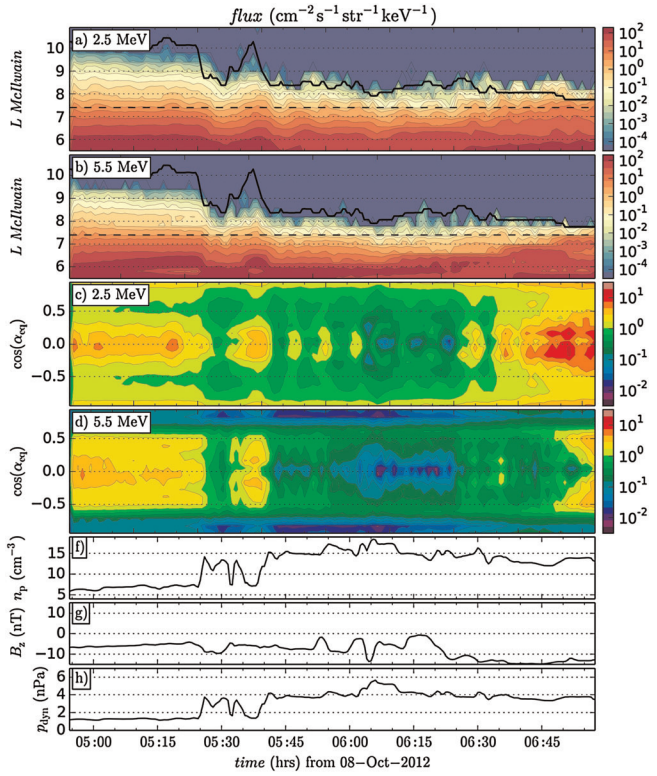

Figure 3. Simulated electron flux following electron guiding centers in LFM-RCM fields. Two energies are shown: (a) 2.5 and (b) 5.5 MeV on 8 October beginning at 5:00 UT. The dashed white line at L = 7.6 is used for computing simulated electron pitch angle distributions following electron guiding centers at (c) 2.5 and (d) 5.5 MeV. Figures 3e, 3f, and 3g are solar wind density, B_z, and dynamic pressure from OMNIWeb. Electron loss penetrates to lower L at higher energy following arrival of the coronal mass ejection shock, while loss of electrons centered on 90° is significantly greater at higher energy. The simulation model follows 1.6 million electron test particles.

Earth's dipole. This was a moderate storm, with minimum Dst = −78 nT on 3 September, and the simulated magnetopause defined in terms of the maximum density gradient compares well with the empirical model. The second storm reached Dst = −133 nT on 1 October, while minimum Dst = −106 nT on 8 October and −111 nT on 9 October, a double-dip storm. Results for these latter two storms are plotted in Figures 2b and 2c, again showing good agreement with the empirical model for magnetopause location for these strong Dst storms (Figure 1). *Lopez et al*. [2007] compared the LFM magnetopause and Shue magnetopause with measurements for the Halloween 2003 storm, validating the accuracy of LFM when the magnetopause comes inside geosynchronous orbit for even more extreme events.

Figures 3a–3b plot simulated electron guiding center flux initially weighted in energy and L by the ESA electron flux model from CRRES measurements [*Vampola*, 1996], shown in 1/(cm^2 s str keV) vs. L-McIlwain, computed from MHD magnetic field line tracing using test particle guiding center trajectories computed in the LFM-RCM fields [*Kress et al*., 2007, 2008]. Two energies are shown: (a) 2.5 and (b) 5.5 MeV on 8 October beginning at 5:00 UT, prior to arrival of the sharp increase in solar wind dynamic pressure ~ 0530 UT. The dashed black line is used to compute simulated electron pitch angle distributions following electron guiding centers at (c) 2–3 and (d) 5–6 MeV. Loss of electrons centered on 90° increases with energy, comparing 2.5 MeV with (d) 5.5 MeV. The greater loss apparent at pitch angles centered on 90°, extending to higher pitch angles at higher energy, is a characteristic signature of magnetopause shadowing [*Turner et al*., 2012, 2013].

4. Discussion

The first storm during the 40-day interval following launch of the Van Allen Probes satellites reached a minimum Dst = −78 nT on 3 September, and the second reached Dst = −133 nT on 1 October. The resulting storage ring feature [*Baker et al*., 2013a] is the remnant outer zone defined by magnetopause loss on 3 September and all but eliminated on 30 September to 1 October. Minimum Dst = −106 nT on 8 October and −111 nT on 9 October. Inward motion of the magnetopause on 3 September and 30 September to 1 October seen in Figures 2a and 2b is consistent with the type of loss simulated for the 8–9 October storm in Figure 3. In terms of integrated flux loss, the second storm was more significant than the first, erasing both the storage ring and reformed outer zone on a timescale much faster than atmospheric loss due to whistler mode hiss, which is thought to maintain the quiet time slot region [*Lyons and Thorne*, 1973; *Thorne et al*., 2013a]. Following recovery from the 1–2 October storm, the outer zone re-emerges inside the model plasmapause in Figure 1, but losses penetrate deeper on 8 October, during the main phase of the first of a double-dip Dst storm. The 8 October depletion occurs during the longest sustained incursion of the magnetopause seen in the three storms simulated in Figure 2, although depth of penetration was not as great as for the other two storms. Simulated ULF wave power in Figure S1 was enhanced inside the magnetopause, beginning with

arrival of the solar wind dynamic pressure increase (~ 0530 UT at the magnetopause), and continued during the period of strongly southward IMF B_Z (Figure 1) through 9 October, when the strong enhancement in flux was observed by REPT (Figure 1). Figure S2 shows that ULF wave power penetrated inside L = 5 following arrival of the increase in solar wind dynamic pressure. The MHD-test particle simulations shown in Figure 3 demonstrate that magnetopause shadowing occurs for 2–6 MeV electrons, most clearly seen in simulated pitch angle distributions with flux minima at 90°. Simulation results indicate the presence of ULF waves which satisfy drift resonance between wave frequencies in the few mHz range [*Elkington et al*., 2003] plotted in Figure S1b. This drift resonance will cause electrons to diffuse and smooth out an inward radial gradient in phase space density associated with a magnetopause incursion [*Shprits et al*., 2006; *Ukhorskiy et al*., 2006]. The energy dependence of the trapped electron pitch angle depletion at 90° evident in Figure 3, stronger at higher energies, is expected from drift shell splitting [*Schulz and Lanzerotti*, 1974] as well as ULF wave contribution to outward radial transport as the magnetopause erodes. Radial diffusion has been shown to be more effective with increasing energy since (magnetic) diffusion coefficients applied to ULF wave fields have an M^2 dependence on first invariant M, accounting for more rapid radial transport for higher energy electrons in a random walk process with a sampling rate tied to the electron drift period [*Fei et al*., 2006].

While magnetopause erosion, drift shell splitting, and ULF wave radial transport can account for loss at higher L values, loss into L = 3 seen in Figure 1 requires an additional mechanism. During the enhanced convection on 8 October, the model plasmapause penetrates inside L = 3, with the strongest plasmapause erosion of the three storms studied. This severe plasmapause erosion then produced conditions conducive to scattering loss by whistler mode chorus at low L values [*Thorne*, 2010] not modeled in this study, which can augment magnetopause loss simulated at higher L values. The rapid acceleration apparent on 9 October [*Reeves et al*., 2013] has been modeled by local acceleration [*Thorne et al*., 2013b], while 3-D test particle simulations of plasmasheet injection in LFM-MIX fields [*Kress et al*., 2014] show that an MeV seed population for local acceleration results from enhanced convection and adiabatic relaxation of the magnetosphere during the northward turning of IMF B_z, around 0800 UT on 9 October (Figure 1). Both of these flux enhancement processes must work against a background of severely depleted trapped electrons on 8 October.

In summary, all three outer zone electron erosion events in Figure 1 coincide with inward motion of the magnetopause in Figure 2 by several R_E, as modeled with the coupled LFM-RCM code. The strong depletion of the outer zone on 8 October, preceding the rapid increase in MeV electron flux on 9 October, tracks magnetopause erosion at higher L during the period of strong solar wind dynamic pressure and subsequent severe plasmapause erosion at lower L. The latter is due to strongly driven convection during the 14-h interval of southward IMF B_z, which begins around 1800 UT on 8 October, after the magnetopause has relaxed (Figure 2c). Thus, depletion of outer zone electrons is influenced by distinct solar wind drivers in close examination of the 8 October depletion event.

Acknowledgments

This work was supported by JHU/APL under NASA's prime contract NAS5-01072, with work at Dartmouth supported under ECT (967399) subcontract from UNH and EFW (922613) subcontract from UMN. The National Center for Atmospheric Research is supported by the National Science Foundation. NSSDC OMNIWeb data were used as input for LFM simulations. Computations were performed on Yellowstone at NCAR and on the Discovery Cluster at Dartmouth. Computations at Rice were supported in part by the Cyberinfrastructure for Computational Research funded by NSF under grant CNS-0821727. We thank Allison Jaynes of the REPT team for preparation of Figure 1.

The Editor thanks three anonymous reviewers for their assistance in evaluating this manuscript.

References

Baker, D. N., et al. (2013a), A long-lived relativistic electron storage ring embedded within the Earth's outer Van Allen Radiation Zone, *Science*, *340*, 186–190, doi:10.1126/science.1233518.

Baker, D. N., et al. (2013b), The Relativistic Electron-Proton Telescope (REPT) Instrument on Board the Radiation Belt Storm Probes (RBSP) Spacecraft: Characterization of Earth's Radiation Belt High-Energy Particle Populations, *Space Sci. Rev.*, *179*, 337–381, doi:10.1007/s11214-012-9950-9.

Bortnik, J., R. M. Thorne, T. O. O'Brien, J. C. Green, R. J. Strangeway, Y. Y. Shprits, and D. N. Baker (2006), Observation of two distinct rapid loss-mechanisms during the November 20th 2003 radiation-belt dropout event, *J. Geophys. Res.*, *111*, A12216, doi:10.1029/2006JA011802.

Elkington, S. R., M. K. Hudson, and A. A. Chan (2003), Resonant acceleration and diffusion of outer zone electrons in an asymmetric geomagnetic field, *J. Geophys. Res.*, *108*(A3), 1116, doi:10.1029/2001JA009202.

Fei, Y., A. A. Chan, S. R. Elkington, and M. Wiltberger (2006), Radial diffusion and MHD-particle simulations of relativistic electron transport by ULF waves in the September 1998 storm, *J. Geophys. Res.*, *111*, A12209, doi:10.1029/2005JA0112112006.

Goldstein, J., J. L. Burch, and B. R. Sandel (2005a), Magnetospheric model of subauroral polarization stream, *J. Geophys. Res.*, *110*, A09222, doi:10.1029/2005JA011135.

Goldstein, J., B. R. Sandel, M. F. Forrester, T. F. Thomsen, and M. R. Hairston (2005b), Global plasmasphere evolution 22–23 April 2001, *J. Geophys. Res.*, *110*, A12218, doi:10.1029/2005JA011282.

Goldstein, J., H. E. Spence, G. D. Reeves, M. F. Thomsen, R. M. Skoug, H. O. Funsten, and R. Livi (2012), Test particle simulation of thermal plasma distribution observed by the HOPE instrument on RBSP-ECT, Abstract SM31C-2363 presented at 2012 Fall Meeting, AGU, San Francisco, Calif., 3-7 Dec.

Hudson, M. K., B. T. Kress, H.-R. Mueller, J. A. Zastrow, and J. Bernard Blake (2008), Relationship of the Van Allen radiation belts to solar wind drivers, *J. Atmos. Sol. Terr. Phys.*, *70*(5), 708–729.

Hudson, M., T. Brito, S. Elkington, B. Kress, Z. Li, and M. Wiltberger (2012), Radiation belt 2D and 3D simulations for CIR-driven storms during Carrington Rotation 2068, *J. Atmos. Sol. Terr. Phys.*, *83*, 51–62.

Kletzing, C. A., et al. (2013), The electric and magnetic field instrument suite and integrated science (EMFISIS) on RBSP, *Space Sci. Rev.*, *179*, 127–181, doi:10.1007/s11214-013-9993-6.

Kress, B. T., M. K. Hudson, M. D. Looper, J. Albert, J. G. Lyon, and C. C. Goodrich (2007), Global MHD test particle simulations of >10 MeV radiation belt electrons during storm sudden commencement, *J. Geophys. Res.*, *112*, A09215, doi:10.1029/2006JA012218.
Kress, B. T., M. K. Hudson, M. D. Looper, J. G. Lyon and C. C. Goodrich (2008), Global MHD test particle simulations of solar energetic electron trapping in the Earth's radiation belts, *J. of Atmos. and Solar-Terr. Phys.*, *70*(14) 1727–1737.
Kress, B. T., M. K. Hudson, and J. Paral (2014), Rebuilding of the Earth's outer electron belt during 8–10 October 2012, *Geophys. Res. Lett.*, *41*, doi:10.1002/2013GL058588.
Li, W., Y. Y. Shprits, and R. M. Thorne (2007), Dynamic evolution of energetic outer zone electrons due to wave-particle interactions during storms, *J. Geophys. Res.*, *112*, A10220, doi:10.1029/2007JA012368.
Lopez, R. E., S. Hernandez, M. Wiltberger, C.-L. Huang, E. L. Kepko, H. Spence, C. C. Goodrich, and J. G. Lyon (2007), Predicting magnetopause crossings at geosynchronous orbit during the Halloween storms, *Space Weather*, *5*, S01005, doi:10.1029/2006SW000222.
Lorentzen, K. R., M. P. McCarthy, G. K. Parks, J. E. Foat, R. M. Millan, D. M. Smith, R. P. Lin, and J. P. Treilhou (2000), Precipitation of relativistic electrons by interaction with electromagnetic ion cyclotron waves, *J. Geophys. Res.*, *105*, 5381–5389, doi:10.1029/1999JA000283.
Loto'aniu, T. M., H. J. Singer, C. L. Waters, V. Angelopoulos, I. R. Mann, S. R. Elkington, and J. W. Bonnell (2010), Relativistic electron loss due to ultralow frequency waves and enhanced outward radial diffusion, *J. Geophys. Res.*, *115*, A12245, doi:10.1029/2010JA015755.
Lyon, J., J. Fedder, and C. Mobarry (2004), The Lyon-Fedder-Mobarry (LFM) global MHD magnetospheric simulation code, *J. Atmos. Sol. Terr. Phys.*, *66*(15-16), 1333–1350, doi:10.1016/j.jastp.2004.03.020.
Lyons, L., and R. Thorne (1973), Equilibrium structure of radiation belt electrons, *J. Geophys. Res.*, *78*(13), 2142–2149.
Merkin, V. G., and J. G. Lyon (2010), Effects of the low-latitude ionospheric boundary condition on the global magnetosphere, *J. Geophys. Res.*, *115*, A10202, doi:10.1029/2010JA015461.
Millan, R. M., and R. M. Thorne (2007), Review of radiation belt relativistic electron losses, *J. Atmos. Sol. Terr. Phys.*, *69*, 362–377.
Millan, R. M., R. P. Lin, D. M. Smith, K. R. Lorentzen, and M. P. Mc- Carthy (2002), X-ray observations of MeV electron precipitation with a balloon- borne germanium spectrometer, *Geophys. Res. Lett.*, *29*(24), 2194, doi:10.1029/2002GL015922.
Millan, R. M., R. P. Lin, D. M. Smith, and M. P. McCarthy (2007), Observation of relativistic electron precipitation during a rapid decrease of trapped relativistic electron flux, *Geophys. Res. Lett.*, *34*, L10101, doi:10.1029/2006GL027718.
O'Brien, T. P., M. D. Looper, and J. B. Blake (2004), Quantification of relativistic electron microbursts during the GEM storms, *J. Geophys. Res.*, *31*, L04802, doi:10.1029/2003GL018621.
Pembroke, A., F. Toffoletto, S. Sazykin, M. Wiltberger, J. Lyon, V. Merkin, and P. Schmitt (2012), Initial results from a dynamic coupled magnetosphere-ionosphere-ring current model, *J. Geophys. Res.*, *117*, A02211, doi:10.1029/2011JA016979.
Reeves, G. D., K. L. McAdams, R. H. W. Friedel, and T. P. O'Brien (2003), Acceleration and loss of relativistic electrons during geomagnetic storms, *Geophys. Res. Lett.*, *30*(10), 1529, doi:10.1029/2002GL106513.
Reeves, G. D., et al. (2013), Electron acceleration in the Heart of the Van Allen Radiation Belts, *Science*, *341*, 991–994, doi:10.1126/science.1237743.
Rostoker, G., S. Skone, and D. N. Baker (1998), On the origin of relativistic electrons in the magnetosphere associated with some geomagnetic storms, *Geophys. Res. Lett.*, *25*(19), 3701–3704, doi:10.1029/98GL02801.
Schulz, M., and L. J. Lanzerotti (1974), *Particle Diffusion in the Radiation Belts*, Physics and Chemistry in Space, vol. 7, Springer-Verlag, New York Heidelberg Berlin.
Selesnick, R. S. (2006), Source and loss rates of radiation belt relativistic electrons during magnetic storms, *J. Geophys. Res.*, *111*, A04210, doi:10.1029/2005JA011473.
Selesnick, R. S., and J. B. Blake (2000), On the source location of radiation belt electrons, *J. Geophys. Res.*, *105*, 2607–2624.
Shprits, Y. Y., R. M. Thorne, R. Friedel, G. D. Reeves, J. Fennell, D. N. Baker, and S. G. Kanekal (2006), Outward radial diffusion driven by losses at magnetopause, *J. Geophys. Res.*, *111*, A11214, doi:10.1029/2006JA011657.
Shprits, Y. Y., S. R. Elkington, N. P. Meredith, and D. A. Subbotin (2008a), Review and sources of relativistic electrons in the outer radation belt: 1 - Radial transport, *J. Atmos. Sol. Terr. Phys.*, *70*, 1694–1713, doi:10.1016/j.jastp.2008.06.014.
Shprits, Y. Y., D. A. Subbotin, N. P. Meredith, and S. R. Elkington (2008b), Review of modeling of losses and sources of relativistic electrons in the outer radiation belt II: Local acceleration and loss, *J. Atmos. Sol. Terr. Phys.*, *70*(14), 1694–1713, doi:10.1016/j.jastp.2008.06.014.
Shue, J.-H., et al. (1998), Magnetopause location under extreme solar wind conditions, *J. Geophys. Res.*, *103*(A8), 17,691–17,700, doi:10.1029/98JA01103.
Summers, D., and R. M. Thorne (2003), Relativistic electron pitch-angle scattering by electromagnetic ion cyclotron waves during geomagnetic storms, *J. Geophys. Res.*, *108*(A4), 1143, doi:10.1029/2002JA009489.
Summers, D., C. Ma, and T. Mukai (2004), Competition between acceleration and loss mechanisms of relativistic electrons during geomagnetic storms, *J. Geophys. Res.*, *109*, A04221, doi:10.1029/2004JA01043.
Summers, D., B. Ni, and N. P. Meredith (2007), Timescales for radiation belt electron acceleration and loss due to resonant wave-particle interactions: 2. Evaluation for vlf chorus, elf hiss, and electromagnetic ion cyclotron waves, *J. Geophys. Res.*, *112*, A04207, doi:10.1029/2006JA011993.
Thorne, R. M. (2010), Radiation belt dynamics: The importance of wave-particle interactions, *Geophys. Res. Lett.*, *37*, L22107, doi:10.1029/2010GL044990.
Thorne, R. M., et al. (2013a), Evolution and slow decay of an unusual isolated ring of relativistic electrons near L~3.2 following the September 2012 magnetic storm, *Geophys. Res. Lett.*, *40*, 3507–3511, doi:10.1002/grl.50627.
Thorne, R. M., et al. (2013b), Rapid local acceleration of relativistic radiation belt electrons by magnetospheric chorus, *Nature*, *504*, 411–414, doi:10.1038/nature12889.
Turner, D. L., Y. Shprits, M. Hartinger, and V. Angelopoulos (2012), Explaining sudden losses of outer radiation belt electrons during geomagnetic storms, *Nat. Phys.*, *8*(3), 208–212, doi:10.1038/nphys2185.
Turner, D. L., V. Angelopoulos, W. Li, M. D. Hartinger, M. Usanova, I. R. Mann, J. Bortnik, and Y. Shprits (2013), On the storm-time evolution of relativistic electron phase space density in Earth's outer radiaztion belt, *J. Geophys. Res. Space Physics*, *118*, 2196–2212, doi:10.1002/jgra.50151.
Ukhorskiy, A. Y., B. J. Anderson, P. C. Brandt, and N. A. Tsyganenko (2006), Storm time evolution of the outer radiation belt: Transport and losses, *J. Geophys. Res.*, *111*, A11S03, doi:10.1029/2006JA011690.
Ukhorskiy, A. Y., M. I. Sitnov, K. Takahashi, and B. J. Anderson (2009), Radial transport of radiation belt electrons due to stormtime Pc5 waves, *Ann. Geophys.*, *27*, 2173–2181.
Vampola, A. L. (1996), The ESA outer zone electron model update, ESA Symp. Proc, in *Environment Modelling for Space-Based Applications*, edited by W. Burke and T.-D. Guyenne, pp. 151–158, ESTEC, Nordwijk, Netherlands.
Wiltberger, M., R. S. Weigel, W. Lotko, and J. A. Fedder (2009), Modeling seasonal variations of auroral particle precipitation in a global-scale magnetosphere-ionosphere simulation, *J. Geophys. Res.*, *114*, 01204, doi:10.1029/2008JA013108.